Materiales de Construcción 75 (360)
October-December 2025, e392
ISSN-L: 0465-2746, eISSN: 1988-3226
https://doi.org/10.3989/mc.2025.399824

Research on the impact of waste rubber particles and polyvinyl alcohol (PVA) fibers on the static mechanical properties and impact resistance of concrete

Z. Luo[a], H. Liu[a], G. Liu[b] ✉

a. School of Civil and Architectural Engineering, Liaoning University of Technology, (Jinzhou, China)
b. School of Civil Engineering and Architecture, NingboTech University, (Ningbo, China)
✉: liugenjin@163.com

Received 2 November 2024
Accepted 21 March 2025
Available on line 15 January 2026

ABSTRACT: This article examines the impact of rubber particles and PVA fibers on concrete's static mechanical properties and impact resistance. It analyzes the mechanism of action through scanning electron microscopy (SEM). The findings demonstrate that as the percentage of rubber particles increases, the compressive strength, flexural strength, and tensile strength of concrete gradually decrease, while the increase in the number of PVA fibers shows a trend of first increasing and then decreasing. When adding 0.15% PVA fibers, the static mechanical properties of concrete are the best. The impact resistance of rubber particles is markedly superior to that of PVA fibers. Compared with normal concrete (NC), adding 0.2% PVA fiber increases the initial and final cracking impact energy (W_1 and W_2) by 82.72% and 83.33%. Furthermore, a 5% rubber particle replacement rate has been found to increase W_1 and W_2 by 154.32% and 157.14%, respectively. The two-parameter Weibull distribution function can effectively describe the impact life evolution of the specimen.

KEY WORDS: PVA fibers reinforced concrete; Rubber particles; Static mechanical properties; Weibull distribution; Impact resistance.

Citation/Citar como: Luo Z, Liu H, Liu G. 2025. Research on the impact of waste rubber particles and polyvinyl alcohol (PVA) fibers on the static mechanical properties and impact resistance of concrete. Mater. Construcc. 75(360):e392. https://doi.org/10.3989/mc.2025.399824

RESUMEN: *Investigación sobre el impacto de las partículas de caucho de desecho y las fibras de alcohol polivinílico (PVA) en las propiedades mecánicas estáticas y la resistencia al impacto del hormigón.* Este artículo examina el impacto de las partículas de caucho y las fibras de PVA en las propiedades mecánicas estáticas y la resistencia al impacto del hormigón, analizando el mecanismo de acción mediante microscopía electrónica de barrido (SEM). Los hallazgos demuestran que a medida que aumenta el porcentaje de partículas de caucho, la resistencia a la compresión, la resistencia a la flexión y la resistencia a la tracción del hormigón disminuyen gradualmente, mientras que el aumento en el número de fibras de PVA muestra una tendencia a aumentar primero y luego disminuir dichas resistencias. Las mejores propiedades mecánicas estáticas del hormigón se logran al añadir un 0.15% de fibras de PVA. La resistencia al impacto de las partículas de caucho es notablemente superior a la de las fibras de PVA. En comparación con el hormigón normal (NC), añadir un 0.2% de fibra de PVA aumenta las energías de impacto inicial y final de fisuración (W_1 y W_2) en un 82.72% y un 83.33%, respectivamente. Además, se ha encontrado que una tasa de reemplazo de partículas de caucho del 5% aumenta W_1 y W_2 en un 154.32% y un 157.14%, respectivamente. La función de distribución de Weibull de dos parámetros puede describir eficazmente la evolución de la vida útil del impacto de la muestra.

PALABRAS CLAVE: Hormigón reforzado con fibras de PVA; Partículas de caucho; Propiedades mecánicas estáticas; Distribución de Weibull; Resistencia al impacto.

1. INTRODUCTION

At present, concrete, as one of the most widely used building materials in practical engineering, has the advantages of easy production, low maintenance, and long service life. As a man-made material, the flexural, tensile, crack resistance, and impact strengths of concrete are often inadequate, despite its high compressive strength (1). Some researchers have found that rubber particles can be added to concrete to improve its plasticity and toughness (2, 3). As a green building material, rubber concrete prepared by mixing rubber particles into concrete has better deformation properties and toughness, impact resistance, and fatigue resistance, as well as realizing the recycling of solid waste, and has been widely used in engineering practice (4-8). However, the addition of rubber particles makes the various strength indicators of concrete significantly lower (9-11), which greatly limits its application in structural engineering (12, 13).

Some scholars have attempted to enhance the mechanical properties of concrete by incorporating PVA fibers. The bridging and crack resistance of PVA fibers can limit the formation and development of microcracks and macrocracks, and significantly enhance the static mechanical properties of concrete (14-16). PVA fibers, as one of the important types of synthetic fibers, have been widely used in various fields due to their high shrinkage resistance, high modulus of elasticity, good corrosion resistance, and freeze-thaw cycling properties (17-20). When mixed into concrete, they not only effectively inhibit concrete cracking but also improve the brittleness and other properties of concrete (21, 22). Noushini (23) et al. and Mondoringin (24) et al. found that incorporating an appropriate amount of PVA fibers into concrete can improve its mechanical properties. When the water-to-cement ratio is 0.4, the optimal amount of PVA fibers is 0.1%. Sagar (25) et al. discovered that the integration of PVA fibers reduced the mix compatibility and the fiber content of 0.3% resulted in the best overall mechanical properties were the best. Cai (26) et al. found through drop-weight impact tests that under the same impact energy, the effect of PVA fiber-reinforced concrete in absorbing impact energy can reach 48 times that of ordinary concrete, and its effect is 9 times that of steel fiber-reinforced concrete. Currently, research on the improvement of concrete mechanical properties by PVA fibers mainly focuses on crack resistance (27), flexural resistance (28-30), and impact resistance (31).

To improve the toughness and strength of concrete, fibers and rubber particles can be added to the concrete simultaneously, such as in steel fiber rubber concrete. Research indicates that adding steel fibers and rubber particles to concrete can significantly improve its static mechanical properties and enhance its impact resistance and ductility, thereby further increasing the durability, toughness, and crack resistance of the concrete (32-34). Abaza et al. (35) found through the study of the flexural load-deformation characteristics of steel fiber rubber concrete that the addition of rubber improved the elastic properties of the concrete, while the incorporation of steel fibers further enhanced the toughness of the concrete. Given the limitations of steel fibers and operating on the same fundamental principles, there must be a corresponding synergistic effect between PVA fibers and rubber particles. However, existing research on this topic is very limited.

Based on the preceding information, 16 distinct mixes were designed, including four PVA fiber mixtures (0%, 0.1%, 0.15%, and 0.2%) and four rubber particle mixtures (0%, 1%, 3%, and 5%). First, PVA fiber-reinforced concrete (PVA-FRC, PFC) was prepared, and the optimal PVA fiber content was determined. On this basis, the compressive strength, flexural strength, tensile strength, impact resistance, and microstructure of the PFC specimens were prepared and tested. The impact life of PFC samples was investigated using the two-parameter Weibull distribution theory, thereby establishing a prediction model and analyzing the intrinsic mechanism of coupling between PVA fibers and rubber particles in PFC samples.

2. EXPERIMENTAL PROCEDURE

2.1. Materials

The cement utilized was Ordinary Portland Cement P.O. 42.5. Table 1 shows the physical property index of the cement. With a range of particle sizes from 5 to 20 mm, an apparent density of 2560 kg/m^3, a bulk density of 1461 kg/m^3, and a crushing index of 8.1% crushed natural stone is used as coarse aggregate. The fine aggregate is river sand, which has a fineness modulus of 2.72, an apparent density of 2643 kg/m^3, and a bulk density of 1726 kg/m^3. To achieve the desired processability, a polycarboxylate-based superplasticizer with a water reduction rate of 28% was added at a dosage of 0.3% to 1.0%. The rubber particles were manufactured by crushing scrap tires, as illustrated in Figure 1. Figure 1 depicts the PVA fibers and their respective properties, presented in Table 2. The physical properties of the rubber particles are presented in Table 3. The water utilized in the mixture was obtained from a municipal tap.

Table 1. Physical property indicators of cement.

Proportion	Specific surface area (m^2/kg)	Stability	Solidification time (min)		Compressive strength (MPa)		Flexural strength (MPa)	
			Initial condensation	Final condensation	3d	28d	3d	28d
3.11	358	Eligible	175	316	24.2	49.5	5.1	8.5

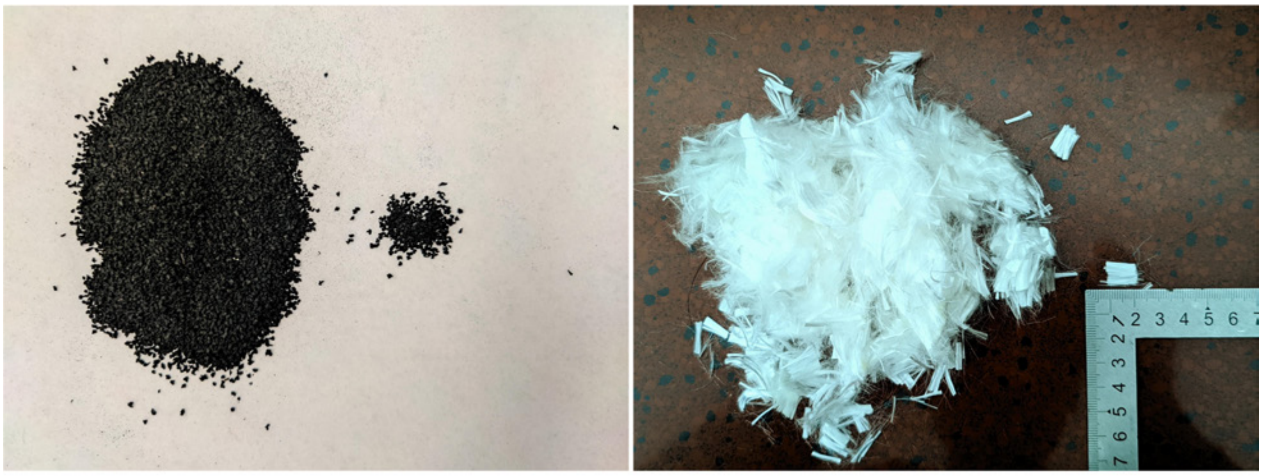

(a) Rubber particles (b) PVA fibers

Figure 1. PVA fibers and rubber particles were used in this test**.**

Table 2. Physical properties of PVA fibers.

Length (mm)	Diameter (μm)	Density (g/cm^3)	Tensile strength (MPa)	Elastic modulus (GPa)	Elongation (%)
12	15.09	1.29	1830	40	6.9

Table 3. Physical properties of Rubber.

Diameter (mm)	Density (kg/m^3)	Heating reduction (%≤)	Ash (%≤)	Iron content (%≤)	Sieve residue (%≤)
0.850	750	0.62	6.75	0.029	0.014

2.2. Concrete mix design

According to JGJ 55-2011 (36), NC mixes of strength class C40 were prepared as control mixes as illustrated in Table 4. Based on NC, PVA fibers were added at 0%, 0.1%, 0.15%, and 0.2% by volume of cement mortar to prepare PFC samples. In addition, rubber particles with substitution rates of 0%, 1%, 3%, and 5% were incorporated to prepare PFC-R samples.

The production of the test specimens follows the standards specified in GB/T50081-2019 (37). A total of 16 sets, comprising 192 test specimens, were prepared. Each set includes 3 cubic samples (150 mm × 150 mm × 150 mm) for measuring cubic compressive strength, 3 cubic samples (100 mm × 100 mm × 100 mm) for measuring splitting tensile strength, 3 prisms (100 mm × 100 mm × 300 mm) for measuring axial compressive strength, and 3 prisms (100 mm × 100 mm × 400 mm) for measuring impact resistance. The specimen preparation process mainly includes adding various materials to a concrete mixer and mixing them evenly in order. The process of specimen preparation mainly includes adding various materials into the concrete mixer in order and mixing them well, loading the mold, vibrating, compaction, smoothing the surface and molding, demolding, and curing. Before testing, all specimens were subjected to a 28-day curing period in a controlled environment at a temperature of 20 ± 5 ºC and a relative humidity exceeding 95%. All specimens were removed and dried 24 hours before testing.

Table 4. Mix proportions of the concrete series (kg/m³).

Types of concrete	Water	Cement	River sand	Natural coarse aggregate	PVA	Rubber particles
NC	185	411	631.00	1195	0	0
PFC0-R1	185	411	624.69	1195	0	6.31
PFC0-R3	185	411	612.07	1195	0	18.93
PFC0-R5	185	411	599.45	1195	0	31.55
PFC0.1	185	411	631.00	1195	1.36	0
PFC0.1-R1	185	411	624.69	1195	1.36	6.31
PFC0.1-R3	185	411	612.07	1195	1.36	18.93
PFC0.1-R5	185	411	599.45	1195	1.36	31.55
PFC0.15	185	411	631.00	1195	2.04	0
PFC0.15-R1	185	411	624.69	1195	2.04	6.31
PFC0.15-R3	185	411	612.07	1195	2.04	18.93
PFC0.15-R5	185	411	599.45	1195	2.04	31.55
PFC0.20	185	411	631.00	1195	2.72	0
PFC0.20-R1	185	411	624.69	1195	2.72	6.31
PFC0.20-R3	185	411	612.07	1195	2.72	18.93
PFC0.20-R5	185	411	599.45	1195	2.72	31.55

Note: NC denotes normal concrete; PFC0-R1 denotes PFC with 1% replacement of rubber granules; and PFC 0.1 denotes PFC with 0.1% PVA fibers blending.

2.3. Test methods

2.3.1. Methods for testing compressive, tensile, and flexural strengths

The test was carried out using a WDW-300KN type electro-hydraulic servo testing machine. According to the requirements of GB/T 50081-2019 (37), each group of 3 specimens, adjusts the loading speed on the control computer and tests Cubic compressive strength and axial compressive strength at a loading speed of 6.0 kN/s and flexural strength at 0.5 kN/s, and test split tensile strength by controlling it within the range of 0.05~0.08 MPa/s range. Throughout the test, it is of the utmost importance to maintain vigilance concerning the overall shape of the specimen. In the event of damage occurring, it is essential to make the necessary adjustments to the instrument on time and to duly record the peak load.

2.3.2. Method to test impact resistance

As illustrated in Figure 2, the specimens were impact tested using a self-designed drop hammer impact test set-up by the American Concrete Institute's (ACI 544 (38)) recommended concrete drop hammer impact test method. The test beam was simply supported at both ends, with an effective span of 300 mm. Before the test, the specimen was placed on the impact test device without eccentricity, and a steel pad was placed at the center of the span on the upper surface of the specimen to moderate the degree of stress concentration on the impact surface. During the test, after the completion of each impact loading, the surface cracking and damage of the specimen were observed. When the first crack appears in the specimen, record the number of impacts at this moment, i.e., the number of impacts of the initial crack ; when the main crack runs through the entire cross-section of the specimen, it is defined as the destruction of the specimen, and record the number of impacts at this moment as the number of destructions . In this paper, we use the number of impacts , the energy absorbed by impact , and the ductility ratio to express the impact resistance of the concrete and the ductility indexes, which are respectively calculated according to Equations [1] and [2].

$$W_i = N_i \cdot mgh \qquad [1]$$

$$\mu = \left(N_2 - N_1\right) / N_1 \qquad [2]$$

Where W_i — he maximum impact energy absorbed by the first and last cracks of different sample groups (J); N_i — number of impacts, divided into N_1 (number of initial cracking impacts) and N_2 (number of final cracking impacts); m — mass of the impact ball, 4.5 kg; g — acceleration of gravity, 9.8 m/s^2; h — impact height, 457 mm.

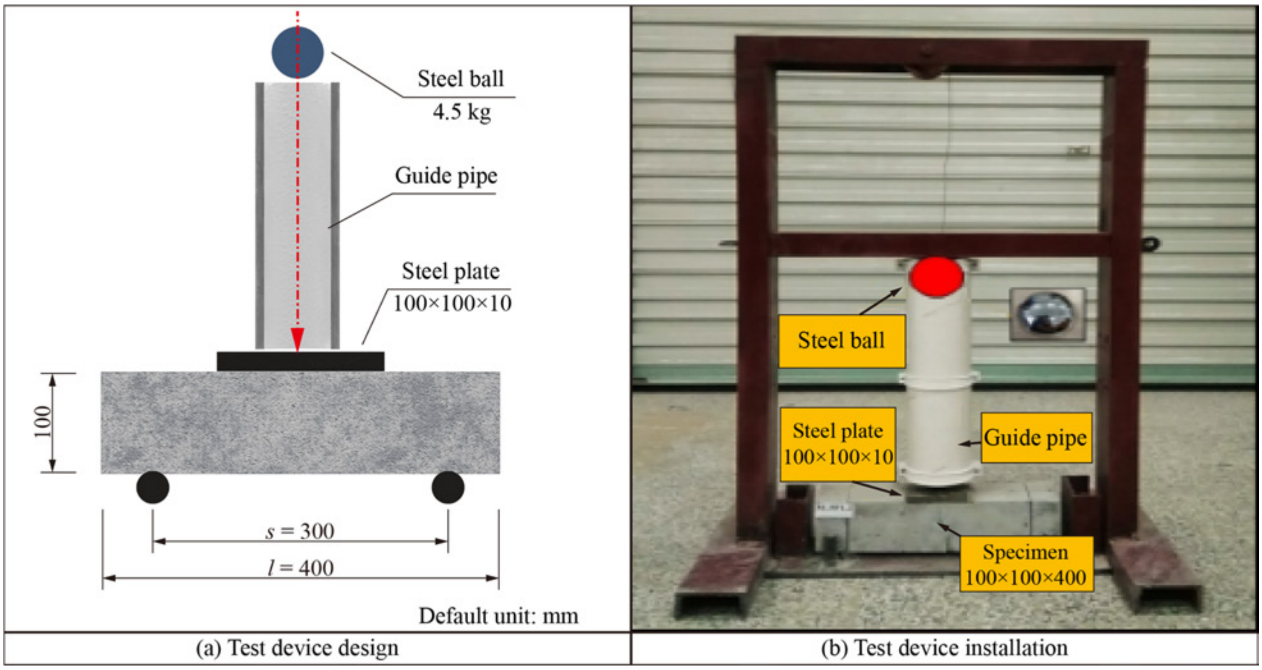

Figure 2. The drop weight impact test device of concrete.

2.3.3. *Microstructure characterization*

A scanning electron microscope model S-3000N manufactured by HITACHI, Japan, was used in this experiment. The scanning electron microscope was used to observe microscopic features such as hydration products, microcracks, and interfacial transition zones in fiber-rubber concrete and to quantify the distribution of microcracks in the interfacial transition zone of the fiber-rubber matrix. The specimens were approximately 10 mm × 10 mm in size and then placed in anhydrous ethanol to prevent continued hydration of the cement stone. Before testing, the specimens were removed from the anhydrous ethanol and dried, placed on an SEM specimen carrier metal sheet coated with conductive adhesive, and then gold-plated using an ion sputtering device.

3. RESULTS AND DISCUSSION

3.1. Static mechanical properties

3.1.1. *Compressive strength*

Table 5 and Figure 3a illustrate the mean compressive strength of the specimens at 28 days. The cubic compressive strength and axial compressive strength of PFC0 exhibited a gradual decline with the increase in rubber substitution rate. The cubic compressive strength of PFC0, PFC0.1, and PFC0.2 exhibited a decline of 4.51%, 11.81%, and 22.52%, respectively, at 1%, 3%, and 5% substitution of rubber particles in comparison to NC. Similarly, the axial compressive strength exhibits a decrease of 2.35%, 5.41%, and 9.41% at the same level of substitution. As the percentage of rubber substitution increased from 0% to 5%, the concrete cubic compressive strength and axial compressive strength of PFC0.15 samples exhibited a decline of 8.50%, 14.05%, and 28.80%, respectively. Axial compressive strength showed a similar downward trend, with a reduction of 9.64%, 5.16%, and 10.76%, respectively. Prior studies have also mentioned this phenomenon (39). Given that the strength of rubber is inferior to that of fine aggregate and that rubber is an organic polymer with elastic properties, whereas the cement matrix is an inorganic material, the properties of the two substances are inherently disparate. The contact surface between rubber and the cementitious matrix is characterized by numerous weak points, which result in relatively poor adhesion and a reduced load-bearing capacity.

As the quantity of PVA fibers increases, the cubic compressive strength and axial compressive strength demonstrate a pattern of initial growth followed by a decline. As the fiber content is increased from 0% to 0.2%, the cubic compressive strength of PFC0, PFC0.1, and PFC0.2 demonstrates an increase of 2.28%, 3.48%, and 2.76%, respectively, in comparison to NC. Similarly, the axial compressive strength exhibited an increase of 2.59%, 4.94%, and 1.41%, respectively. When the specimen is compressed, the bridging effect of PVA fibers allows them to withstand the compressive stress associated with cracking development, reducing lateral deformation and increasing compressive strength. PVA fibers are spread randomly and systematically across the cement paste and aggregates, providing a spatial network that prevents cracking. PVA fibers fill the matrix's major pores, when combined with aggregates, improving compressive strength. Furthermore, excessive fiber diversity could cause flaws in the matrix by causing fiber grouping. This occurrence has resulted in a decrease in the performance of the PFC0.20 sample compared to the PFC0.15 sample.

3.1.2. Flexural strength

The flexural strength results are demonstrated in Table 5 and Figure 3b. With increasing PVA fiber doping, the flexural strength of the samples increases and then decreases. The maximum strength of 6.75 MPa is obtained for PFC0.15; the strengths of PFC0.10, PFC0.15, and PFC0.20 are increased by 1.8%, 2.9%, and 1%, respectively, as compared to that of NC. The PVA fibers have a strong holding power with cement matrix, good affinity to concrete material, and good dispersion. Therefore, it can be connected to fill the pore cracks, uniformly distributed in the concrete and the common force, while the three-dimensional distribution of fibers changes the crack expansion path so that the specimen's internal tensile stress redistribution, thereby improving the specimen's flexural capacity.

As the rate of rubber aggregate substitution increased, a corresponding decrease in flexural strength was observed. The flexural strength of PFC0 concrete exhibited a decline of 1.22%, 4.12%, and 8.84%, respectively, in comparison to NC when the rubber admixture was increased from 0 to 5%. The flexural strength of the PFC0.15 specimens exhibited a notable decline when the rubber mixing amount was increased from 0 to 5%. This decline was observed in all three specimens, with the PFC0.15-R1, PFC0.15-R3, and PFC0.15-R5 specimens displaying a reduction of 13.78%, 3.41%, and 6.96%, respectively. The air-entraining effect of rubber results in an increase in air content within the specimen with an increase in rubber content (40). This reduction in compactness, coupled with the low strength of the rubber material itself, leads to a reduction in bearing capacity and bonding ability with cement mortar. The presence of weak surfaces between the rubber and cement mortar also contributes to a reduction in flexural strength. The findings indicate that incorporating an optimal dosage of PVA fibers into rubber concrete can effectively mitigate the detrimental impact of rubber particles on the flexural strength of concrete.

Table 5. The static mechanical properties of each mixture at 28 days (MPa).

ID	Cubic compressive strength	Axial compressive strength	Flexural strength	Splitting tensile strengths
NC	52.08	42.5	6.56	4.93
PFC0-R1	49.73	41.5	6.48	4.78
PFC0-R3	45.93	40.2	6.29	4.55
PFC0-R5	40.35	38.5	5.98	4.23
PFC0.1	53.27	43.6	6.68	5.29
PFC0.1-R1	50.74	42.9	6.62	5.08
PFC0.1-R3	42.94	39.2	5.79	4.35
PFC0.1-R5	39.08	38.9	6.15	4.38
PFC0.15	53.89	44.6	6.75	5.62
PFC0.15-R1	49.31	40.3	5.82	4.62
PFC0.15-R3	46.32	42.3	6.52	4.68
PFC0.15-R5	38.37	39.8	6.28	4.56
PFC0.20	53.52	43.1	6.62	5.37
PFC0.20-R1	49.36	40.6	6.52	4.72
PFC0.20-R3	44.45	39.5	6.05	4.49
PFC0.20-R5	41.29	39.2	6.18	4.58

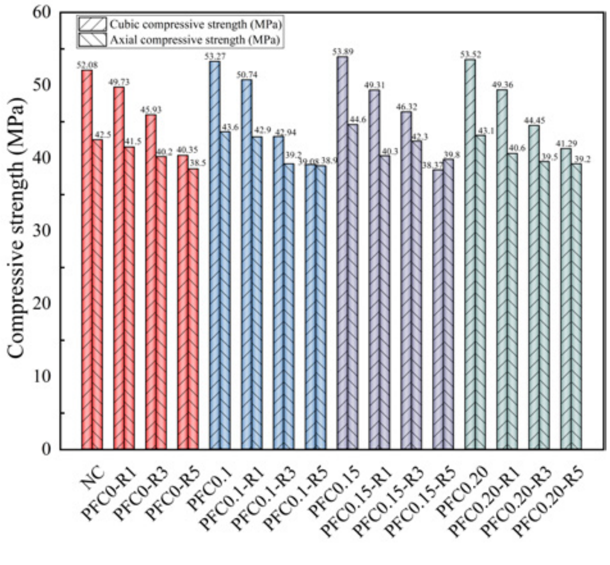

(a) Compressive strength.

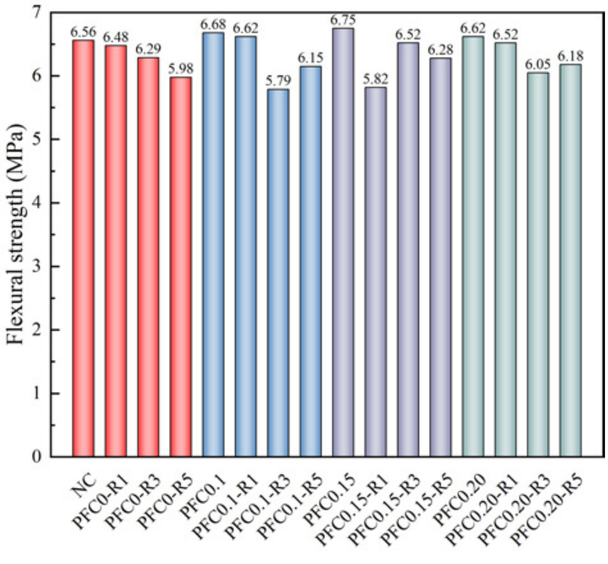

(b) Flexural strength.

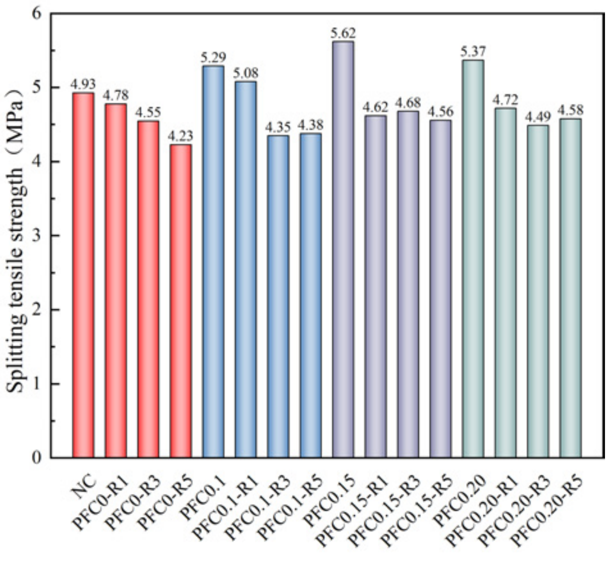

(c) Split tensile strength.

Figure 3. Static mechanical properties of specimen at 28 days.

3.1.3. Splitting tensile strength

Table 5 and Figure 3c illustrates that the splitting tensile strengths of the specimens exhibit a gradual decline with an increase in the rubber substitution rate. In comparison to the NC specimens, the split tensile strengths of the PFC0-R1, PFC0-R3, and PFC0-R5 specimens exhibited a reduction of 3%, 7.71%, and 14.2%, respectively, at rubber substitution rates of 1%, 3%, and 5%. The reduction in specimen strength was more pronounced when the rubber substitution rate was 5%. The observation of the PFC0.15 specimens revealed a decrease in split tensile strength, with the PFC0.15-R1, PFC0.15-R3, and PFC0.15-R5 specimens exhibiting a reduction of 17.79%, 16.73%, and 18.86%, respectively, as the rubber component grew from 0 to 5%. This is due to the hydrophobic nature of rubber, which impairs its ability to combine with other materials during the mixing process. The resulting contact surface bonding performance is inadequate, leading to a notable reduction in strength with an increase in rubber substitution rate.

As the content of PVA fibers incorporated into the specimen increases, the splitting tensile strength exhibits a trend of initial growth followed by a subsequent decline. When the PVA fiber doping level is 0.15%, the splitting tensile strength of the PFC0.15 specimen is 5.62 MPa, which is 12.28% higher than that of the NC specimen.

Conversely, the split tensile strength of the PFC0.20 specimen was observed to be 4.45% lower than that of the PFC0.15 specimen. This is because the fiber can serve as a bridging role, thereby inhibiting the development of cracks when they occur. Nevertheless, when the PVA fibers are excessive, they can readily interlock with one another within the concrete, which ultimately results in a decline in strength.

3.2. Impact resistance tests

3.2.1. Failure modes

Figure 4 illustrates the damage patterns of the samples after impact. As illustrated in Figure 4a, there is only one radial serrated main crack on the surface of the NC specimen. This crack quickly penetrated through the specimen after its appearance, splitting the specimen into two halves, which is a clear case of brittle impact damage. Figure 4b PFC0-R3 sample, although radial cracks also appeared after impact, the initial crack impact count was significantly higher than that of NC. This indicates that the rubber's deformation resistance played a role before the sample cracked. However, since rubber is a hydrophobic material, its bonding with cementitious stone is poor, and when cracks occur in the sample, they will quickly penetrate through. Figure 4c PFC0.15-R3 specimen: due to the combined action of PVA fibers and rubber particles, the initial crack is narrow and weak. As the number of impacts increases, the main crack begins to extend radially until it penetrates the entire specimen. PVA fibers can bridge the specimens between cracks and prevent the formation of cracks.

(a) NC (b) PFC0-R3 (c) PFC0.15-R3

FIGURE 4. Specimen failure impact pattern.

3.2.2. Impact resistance test findings

The impact test results and impact ductility ratios of fiber concrete are presented in Table 6. Table 6 display that the fiber-rubber concrete holds greater initial cracking impact resistance, ultimately cracking impact resistance and ductility ratios than NC.

Figures 5-7 show the relevant impact performance metrics, including the number of impacts (N_1, N_2), energy absorbed by initial and final cracking impact (W_1, W_2), toughness ratio (μ), and number of post-cracking impacts (N_2-N_1). The addition of PVA fibers improves the impact performance of PFC. The rubber and PVA fibers mixtures produced a synergistic effect, the incremental impact energy consumption of the mixtures was higher than that of the single mixtures, and the final cracking impact energy consumption of the specimens of group PFC0.20-R5 increased by 40.5% compared to the specimens of group PFC0.20, and 68.75% compared to that of the specimens of group PFC0-R5, which showed a positive mixing effect. The reason for this is that the PVA fibers themselves have a high modulus of elasticity, which enhances the impact resistance of the concrete and increases the number of impact cracks. Rubber powder can fill the tiny pores in the concrete, increase the compactness of concrete, rubber, and cement matrix synergistic resistance to impact loading, but also give full play to its elasticity, improve the deformation capacity of concrete after impact cracking, enhance the ductility and toughness of concrete, making it more resistant to impact. The N_1 and N_2 of PFC0.20-R5 group specimens were the highest, 69 and 72, respectively, which were 154.3% and 157.1% higher than those of the NC group, respectively. μ of PFC0.15-R3 group specimens was the largest.

Looking at the impact of PVA fibers alone, fiber rubber concrete N_1 and N_2, μ with the increase in fiber mixing, 0.15% is the optimal mixing amount. The appropriate amount of PVA fibers have a good bond with concrete and their high tensile strength, consumes impact energy through bridging deformation and improves impact resistance.

Table 6. Analysis of impact resistance test results.

ID	Average number of blows		N_2-N_1	W_1/W_2 (J)	W_1 increment /W_2 increment (%)	(%)
	N_1	N_2				
NC	27	28	1	544.15/564.30	/	3.70
PFC0-R1	34	36	2	685.23/718.82	25.93/27.38	4.90
PFC0-R3	40	41	1	812.87/826.30	49.38/46.43	1.65
PFC0-R5	42	43	1	846.46/859.89	37.19/35.77	1.59
PFC0.1	34	36	2	678.51/725.53	24.69/28.57	6.93
PFC0.1-R1	44	46	2	880.04/920.35	61.73/63.10	4.58
PFC0.1-R3	45	47	2	900.20/947.22	65.43/67.86	5.22
PFC0.1-R5	50	53	3	1014.40/1068.15	86.42/89.29	5.30
PFC0.15	42	44	2	846.46/886.76	55.56/57.14	4.76
PFC0.15-R1	49	51	2	980.81/1034.56	81.48/83.33	4.76
PFC0.15-R3	54	57	3	1088.30/1148.76	100.00/103.57	5.56
PFC0.15-R5	60	62	2	1202.50/1249.53	120.99/121.43	3.91
PFC0.20	49	51	2	994.25/1034.56	82.72/83.33	4.05
PFC0.20-R1	53	54	1	1061.43/1088.30	95.06/92.86	2.53
PFC0.20-R3	63	66	2	1276.40/1323.43	134.57/134.52	3.68
PFC0.20-R5	69	72	3	1383.89/1451.07	154.32/157.14	4.85

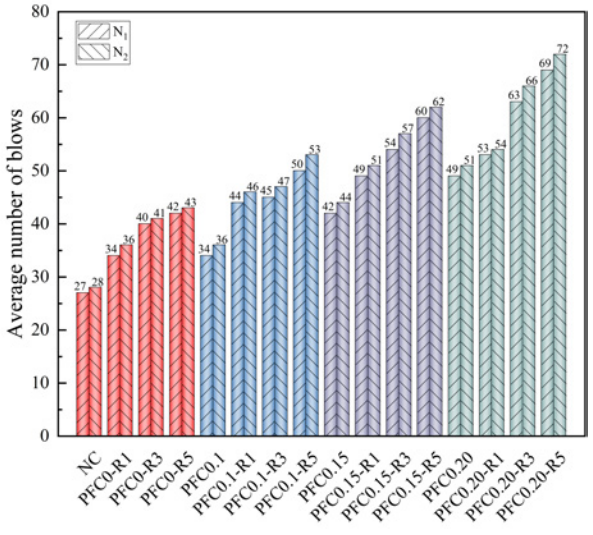

Figure 5. The average number of blows of different concrete specimens.

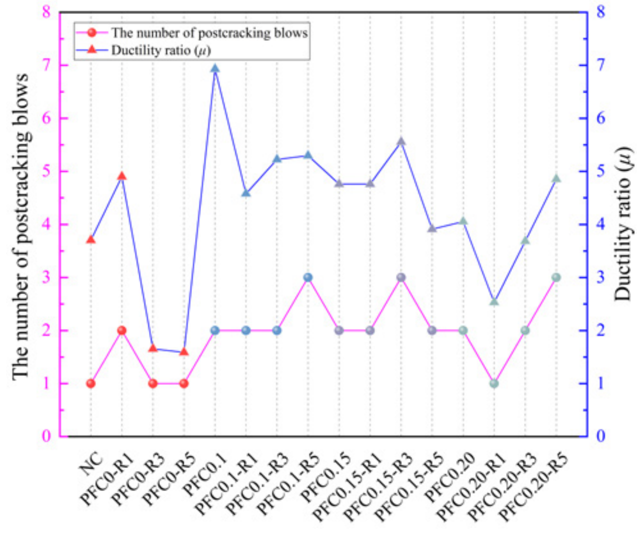

Figure 6. The variation in the number of postcracking impact blows and ductility ratio.

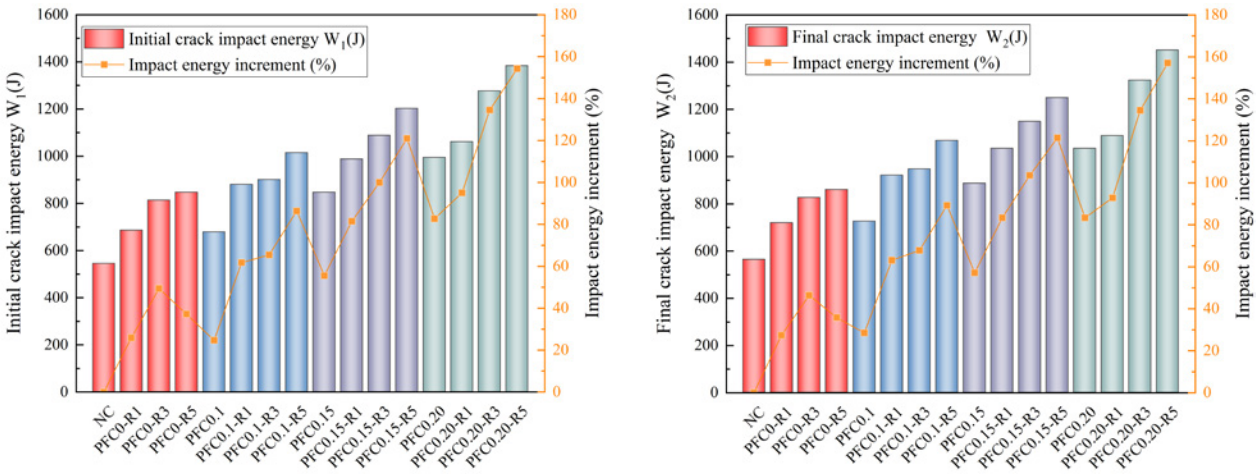

Figure 7. Impact energy and its increment for fiber-rubber concrete.

3.3. Weibull distribution

3.3.1. Theory

From the experimental data in the previous section, it is known that the number of shocks is discrete and random, which is likewise confirmed by many researchers (41, 42). To study the damage law of the impact resistance test more objectively, finding a probability distribution model applicable to the number of impacts has become a research focus. After previous studies, it was found that the damage mechanism of the concrete impact test is highly similar to fatigue damage, so to explore the distribution law of the impact resistance of fiber concrete, the researcher applies the Weibull distribution function to the impact test. After previous studies, it was found that the Weibull distribution function is consistent with the damage properties of concrete materials under impact dynamic loading. In recent years, the Weibull distribution has been widely used in concrete; it can effectively describe the change of failure probability with time and use the test data to derive the correct impact law. Therefore, in this chapter, the Weibull distribution function in the theory related to mathematical statistics is used to fit the analysis and life reliability prediction of the number of initial and final cracking impacts of fiber-rubber concrete, respectively. The Weibull-distributed probability density function of the number of impacts N_x for fiber concrete is expressed as follows:

$$f\left(N_x\right)=\frac{\alpha}{N_a-N_0}\left(\frac{N_x-N_0}{N_a-N_0}\right)^{\alpha-1}\exp\left(\frac{N_x-N_0}{N_a-N_0}\right)^{\alpha} \quad [3]$$

Where: α is the shape parameter of the Weibull distribution; N_a is the scale parameter (characteristic lifetime parameter), >0; N_0 is the position parameter (minimum lifetime parameter), ≥0; N_x is the observed value of the random variable, referring to the number of initial cracking impacts N_1 and the number of final cracking impacts N_2.

The image of the Weibull distribution probability density function is shown in Figure 8. When $\alpha = 1$, the image becomes an exponential distribution function, when $\alpha = 2$, the image becomes a Rayleigh distribution function, and when $3 < \alpha < 5$, the image is close to a normal distribution curve.

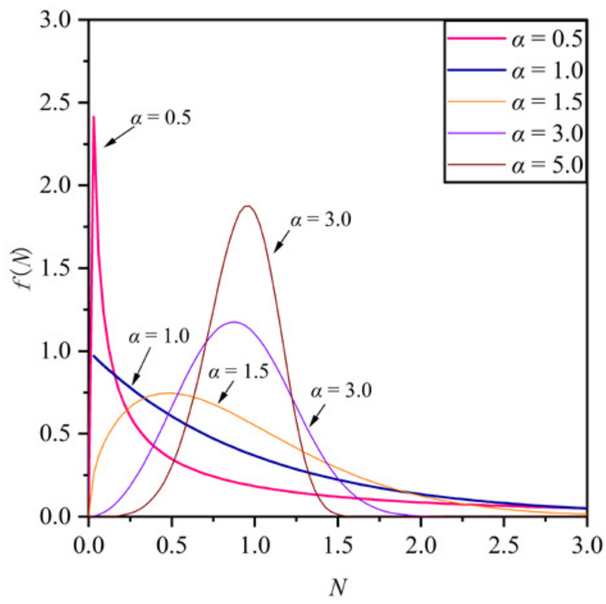

FIGURE 8. Weibull distribution function probability density curve.

Weibull cumulative distribution (probability of failure) function:

$$FN_x = N_0 < N < N_x = 1-\exp\left[-\left(\frac{N_x-N_0}{N_a-N_0}\right)^{\alpha}\right] \quad [4]$$

The survival probability function can be expressed as shown below:

$$P(N_x) = 1 - F(N_x) = \exp\left[-\left(\frac{N_x - N_0}{N_a - N_0}\right)^{\alpha}\right] \qquad [5]$$

From the point of view of safety and reliability, it can be assumed that $N_0 = 0$. Equations [3], [4] and [5] are simplified as follows:

$$f(N_x) = \frac{\alpha}{N_a}\left(\frac{N_x}{N_a}\right)^{\alpha-1} \exp\left[-\left(\frac{N_x}{N_a}\right)^{\alpha}\right] \qquad [6]$$

$$F(N_x) = P(0 < N < N_x) = 1 - \exp\left[-\left(\frac{N_x}{N_a}\right)^{\alpha}\right] \qquad [7]$$

$$P(N_x) = 1 - F(N_x) = \exp\left[-\left(\frac{N_x}{N_a}\right)^{\alpha}\right] \qquad [8]$$

Upon taking the natural logarithm of both sides of Equation [8] twice yields the following equation.

$$\ln\left[\ln\left(\frac{1}{P(N_x)}\right)\right] = \alpha\ln(N_x) - \alpha\ln(N_a) \qquad [9]$$

Let $Y = \ln\left[\ln\left(1/P(N_x)\right)\right]$, $X = \ln N_x$, $\beta = \alpha\ln N_a$ Can be obtained:

$$Y = \alpha X - \beta \qquad [10]$$

If X and Y satisfy the linear equation in the above equation, then the impact life N is demonstrated to conform to a two-parameter Weibull distribution. Mathematical statistics correlation theory (43) says that the coefficient of determination R^2 above 0.7 indicates a good correlation; from the size of the correlation coefficient R to determine the correlation relationship, it is considered that $0.5 < |R| < 0.8$ for the dominant linear correlation, and $|R| > 0.8$ is generally referred to as highly linear correlation.

The initial cracking impact times N_1 and destructive impact times N_2 of each group of concrete specimens were arranged in the order of smallest to largest, respectively, and then the expected valuation of the survival probability function Equation [11] was used to calculate the survival probability:

$$PN_x = 1 - \frac{i}{n+1} \qquad [11]$$

Where i is the number of orders after the number of impacts in order, $i = 1, 2, 3, ..., n$. n is the total number of samples for each group of specimens, this test $n = 3$.

3.3.2. Fitting analysis of impact test findings

According to Equations [9-11] and impact test results, the initial and final cracking impact numbers of the fiber-rubber concrete were fitted to obtain the corresponding parameter values α, β and the correlation coefficient R^2, as shown in Table 7. Figure 9 show the linearly fitted images of the Weibull distribution for the initial and final cracking impact numbers of the specimens.

In this test, R^2 is 0.689 at minimum and 0.997 at maximum, and the coefficient of determination R^2 of most of the specimens reaches above 0.800, which shows that there is a strong linear link between $X=\ln N_x$ and $Y=\ln[\ln(1/P(N_x))]$. Therefore, it can be inferred that the number of impacts of fiber-rubber concrete specimens can obey the two-parameter Weibull distribution function well.

3.3.3. Reliability analysis of impact life

By Equations [8-10] the value of N under different failure probabilities can be calculated using the following equation:

$$N = \exp\left\{ \frac{\ln\ln\left(\frac{1}{1-F\left(N_x\right)} \right) + \beta}{\alpha} \right\} \quad [12]$$

Table 7. Weibull distribution linear fitting parameter.

ID	N_1			N_2		
	α	β	R^2	α	β	R^2
NC	7.608	25.479	0.858	7.883	26.672	0.858
PFC0-R1	9.531	34.019	0.856	8.257	29.923	0.689
PFC0-R3	20.276	75.383	0.939	15.664	58.589	0.689
PFC0-R5	8.841	33.450	0.963	7.673	29.205	0.948
PFC0.1	8.540	30.437	0.945	7.664	27.868	0.919
PFC0.1-R1	15.735	59.840	0.889	16.447	62.265	0.889
PFC0.1-R3	-50.409	-191.085	0.689	36.963	142.736	0.996
PFC0.1-R5	11.403	45.099	0.828	14.745	58.959	0.853
PFC0.15	10.998	41.524	0.997	12.276	46.868	0.854
PFC0.15-R1	5.174	20.531	0.826	5.732	22.971	0.885
PFC0.15-R3	6.309	25.571	0.769	8.020	32.832	0.858
PFC0.15-R5	5.529	24.237	0.757	6.498	27.219	0.823
PFC0.20	11.011	43.339	0.983	15.906	63.060	0.971
PFC0.20-R1	10.041	40.216	0.810	10.374	41.797	0.689
PFC0.20-R3	14.123	59.000	0.982	12.638	53.298	0.962
PFC0.20-R5	10.664	45.512	0.974	11.315	48.801	0.997

Combined with the regression fitting coefficients α and β in Table 7, the specific values of P for the failure probability function F(N_x) are taken as 5%, 15%, and 30%, respectively, and the predicted values of the initial and final cracking impact life of each group of specimens under different failure probabilities can be obtained, as shown in Table 8. Then the natural logarithm is taken to obtain lnN_1 and lnN_2, and the line graphs of the impact life of each group at varying failure probabilities are constructed, as illustrated in Figure 10. As the content of PVA fiber and rubber particles increases, the expected impact life for both initial and final cracks is enhanced for each group, which is consistent with the experimental results at the same failure probability.

Table 8. Impact the life of samples with various failure probabilities.

ID	Failure Probability					
	N_1			N_2		
	5%	**15%**	**30%**	**5%**	**15%**	**30%**
NC	19	22	25	20	23	26
PFC0-R1	26	29	32	26	30	33
PFC0-R3	36	38	39	35	38	39
PFC0-R5	31	36	39	31	35	39
PFC0.1	25	29	31	26	30	33
PFC0.1-R1	37	40	42	37	39	41
PFC0.1-R3	47	46	45	44	45	46
PFC0.1-R5	40	45	48	45	48	51
PFC0.15	33	37	40	36	39	42
PFC0.15-R1	30	37	43	33	40	46
PFC0.15-R3	36	43	49	41	48	53
PFC0.15-R5	47	58	66	42	50	56
PFC0.20	39	43	47	44	47	49
PFC0.20-R1	41	46	50	42	47	51
PFC0.20-R3	53	57	61	54	59	63
PFC0.20-R5	54	60	65	57	64	68

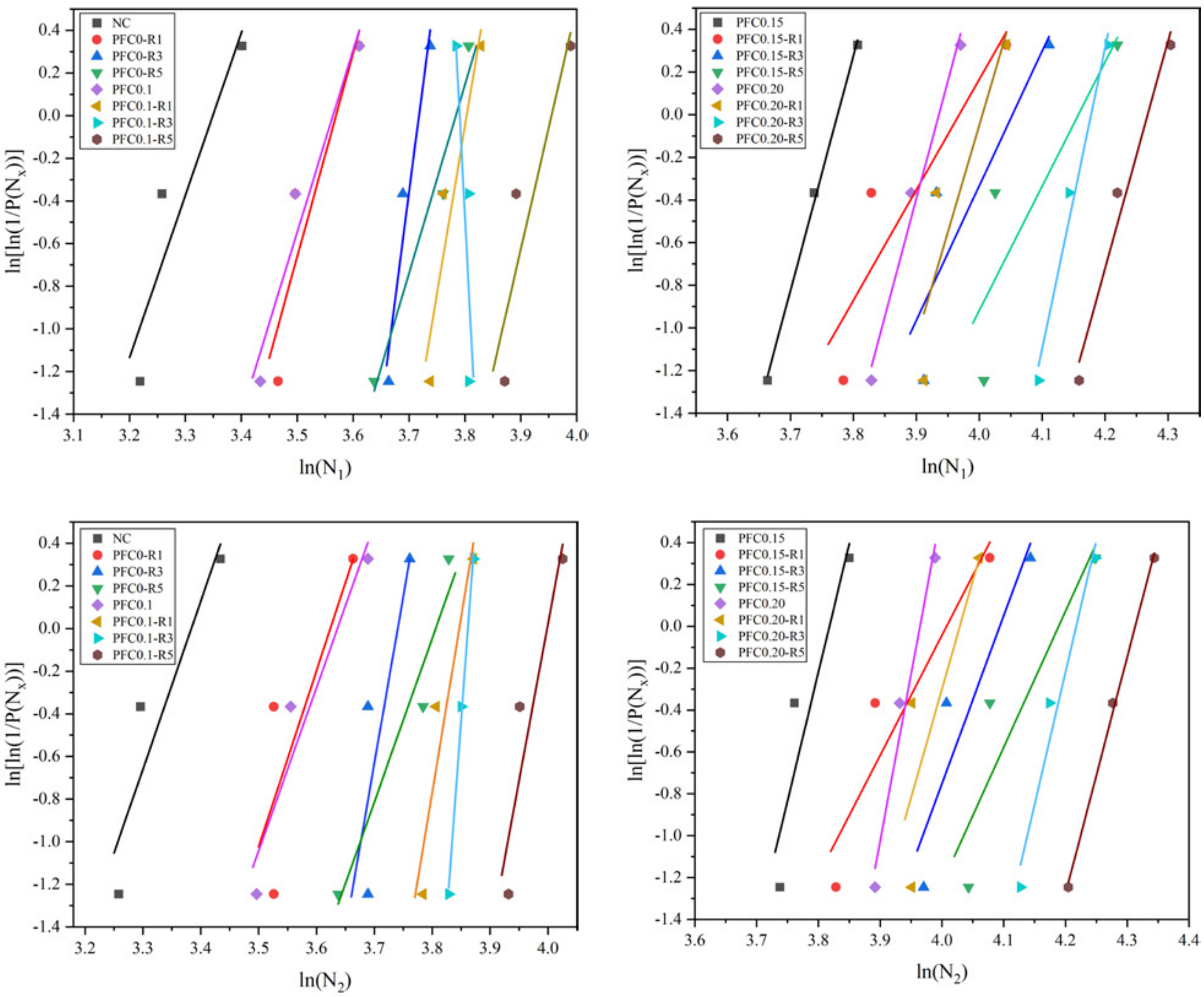

FIGURE 9. N_1 and N_2 linear fit curves.

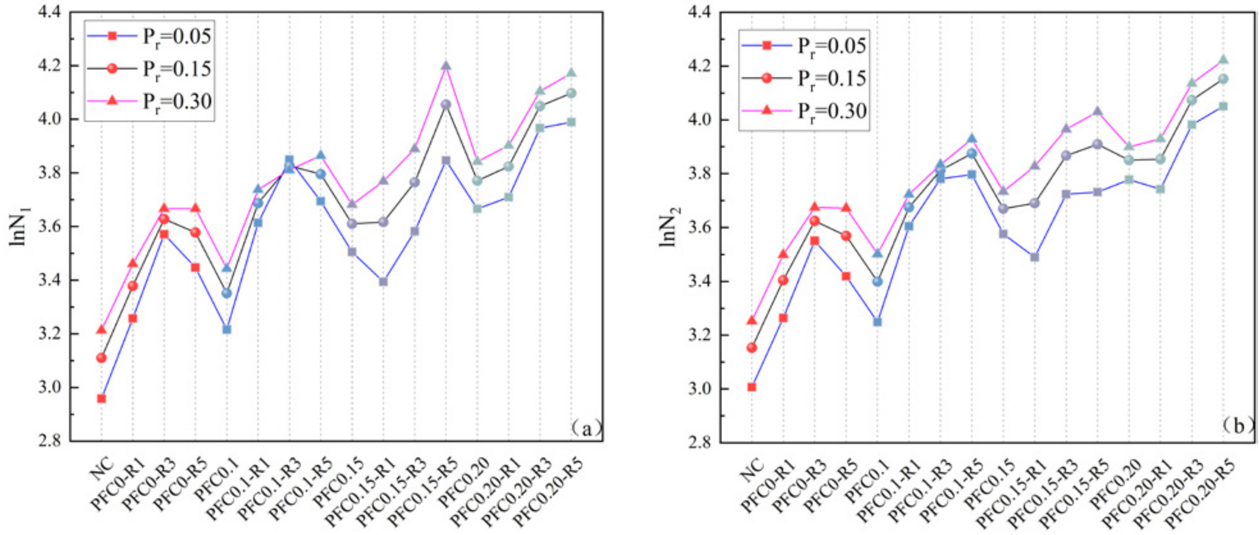

FIGURE 10. Line diagram of impact life of fiber-rubber concrete for different failure probabilities.

3.4. Microstructure analysis

3.4.1. Micro-morphological analysis of specimens

Figure 11 depicts the micro-morphological photographs of the NC, PFC0.15, PFC0.2-R3, and PFC0.20-R5 specimens. As illustrated in the figure, there are many defects and harmful pores in the cement-hardened paste in the NC specimen (Figure 11a). PVA fibers are evenly distributed on the cement soil surface of the PFC0.15, PFC0.20-R3, and PFC0.20-R5 specimens. Due to the bridging effect of the fibers, the PVA fibers are effectively bonded to the mortar interface to form a micro-reinforcement system, which is beneficial to the bending toughness of the specimens (Figure 11b, 11c and 11d). The rubber particles are randomly dispersed in the concrete matrix and evenly distributed in the mortar matrix. The amount of rubber particles can be appropriately increased. The rubber powder can fill some small pores in the concrete, thereby improving the toughness of the concrete (Figure 11c and 11d). However, rubber is an organic material with poor compatibility. With the increase in rubber content, the amount of bubbles introduced into the concrete increases, and the pores inside the concrete increase, which leads to a decrease in the compressive strength of the concrete.

3.4.2. Microscopic analysis of the rubber-mortar interface ITZ

Figure 12 illustrates the morphology of hydration products in the interfacial transition zone (ITZ) of the rubber-mortar matrix interface numbered PFC0.2-5. It can be observed that a small number of short columnar and clustered C-S-H and a considerable number of CH crystals (square or rectangular) are generated inside the mortar. CH has low strength and poor stability, while C-S-H gel can connect various hydration products to form a three-dimensional spatial structure (44). The formation of short columnar and clustered C-S-H leads to an increase in the volume of hydration products. Due to the small number of C-S-H, the pore volume between the rubber and mortar matrix interface is increased, making the hydration products show a relatively void structure, thereby reducing the ITZ strength of PFC0.2-R5.

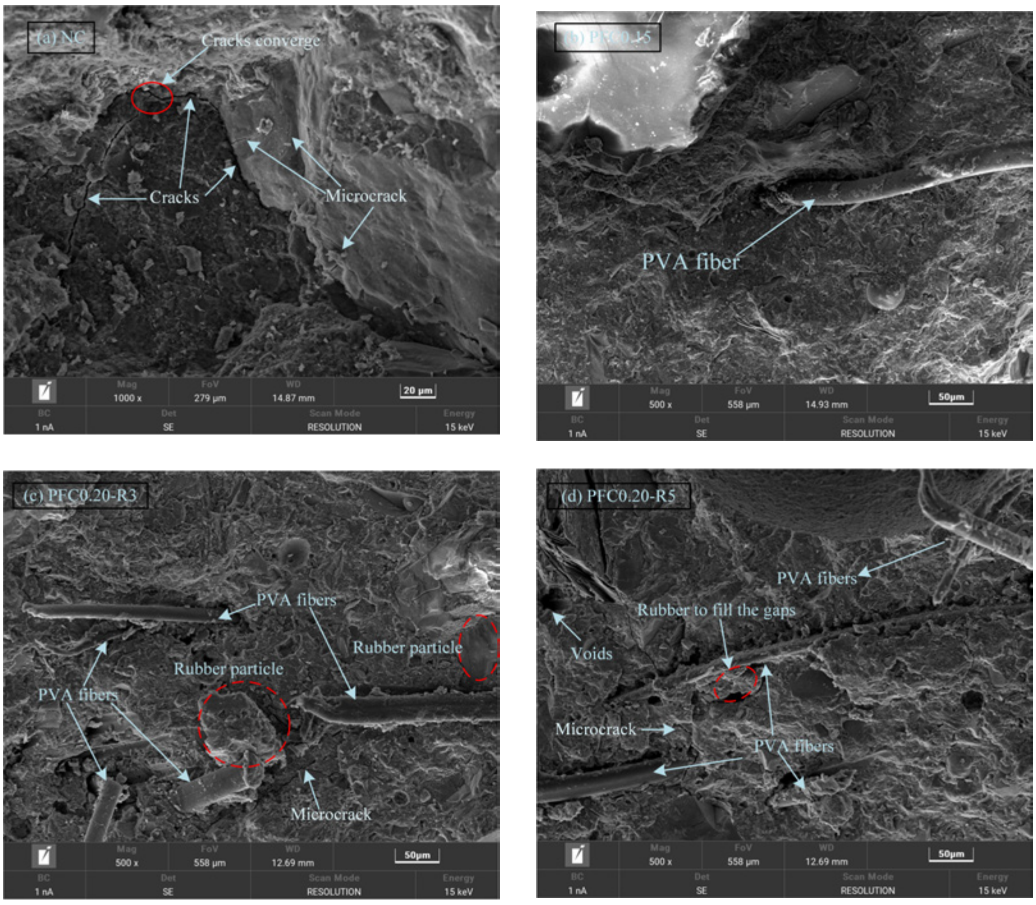

FIGURE 11. SEM photographs for specimen.

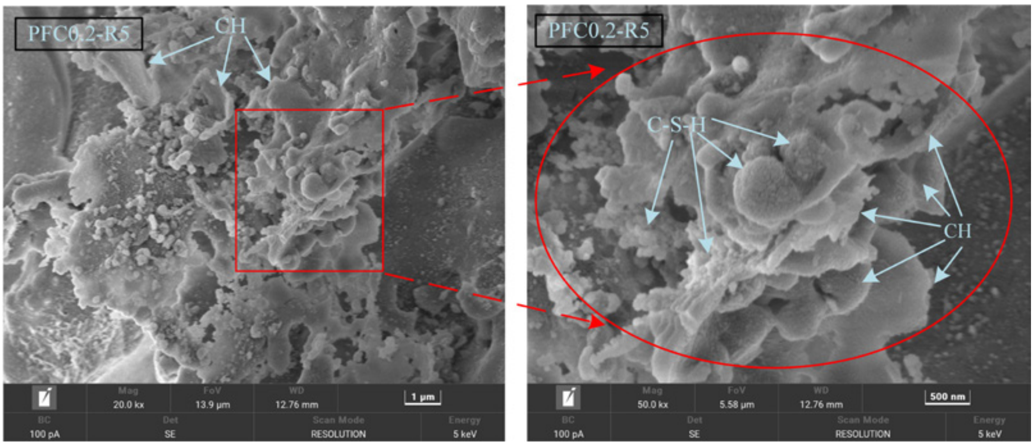

Figure 12. Hydration product morphology at the ITZ of rubber-mortar interface.

3.4.3. Analysis of the mechanism of crack-resistant reinforcement of PVA fibers

PVA fibers exhibit a three-dimensional random distribution in concrete, forming a spatial network that enhances the overall load transfer performance. As illustrated in Figure 13, PVA fibers primarily bond and work synergistically with concrete in two ways: one is that PVA fibers effectively prevent cracking; the other is that the chemical bonding force between the surface of the PVA fibers and the concrete transmits stress to the matrix on both sides of the crack while consuming some of the stress for the tensile deformation failure of the fibers themselves, thereby preventing further crack propagation, enhancing their tensile performance, and thereby improving flexural strength and impact resistance.

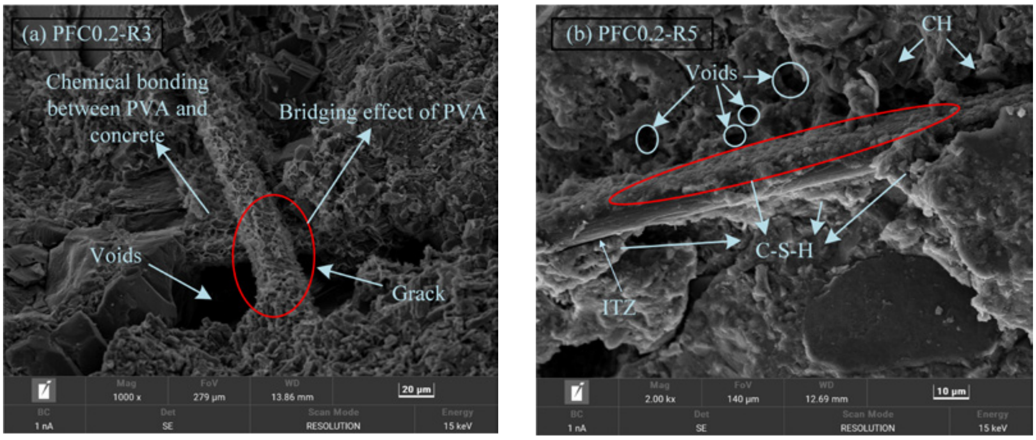

Figure 13. Crack resistance mechanism of PVA fibers.

4. CONCLUSIONS

This study aimed to investigate the effect of PVA fibers and rubber particles on the mechanical properties and impact resistance of concrete. The principal findings are as follows:

1. The compressive strength, axial compressive strength, flexural strength, and splitting tensile strength of the cube decrease with the increase in the replacement rate of rubber particles. However, as the PVA fiber content increases, the strength initially increases and then decreases. When the PVA fiber content is 0.15%, the static mechanical properties of the specimen are the best, with strength increases of 3.48%, 4.94%, 2.9%, and 12.28%.
2. The impact resistance notably increased in correlation with the elevation in PVA fibers and rubber particle content. An increase in PVA fibers doping from 0 to 0.2% resulted in a 200% increase in N_2-N_1, an 82.72% increase in W_1, and an 83.33% increase in W_2. An increase in rubber particle substitution from 0 to 5% resulted in a 200% increase in N_2-N_1, a 120.99% increase in W_1, and a 121.43% increase in W_2. The results of the impact tests exhibited a two-parameter Weibull distribution.

3. Microscopic analysis indicates that PVA fibers enhance the mechanical properties of concrete through their effective crack resistance, the chemical bonding with concrete, and the bridging effect of the PVA fibers. This confirms the claim that PVA fibers can enhance the mechanical properties of concrete. The mechanical interaction between rubber particles and the matrix will gradually reduce the strength of the concrete and increase its deformability.

Furthermore, in consideration of the constraints inherent to the subject matter of this study and the extant research findings, some prospects for future research may be: PFC exhibits excellent mechanical properties and toughness, making it a promising candidate for use in bridge components, airport runways, and other infrastructure applications. However, these works are predominantly vulnerable to rapid fluctuations and the effects of cyclic stresses, which raises the issue of fatigue resistance. Furthermore, the fracture properties and cracking process of PFC under impact loading remain a topic worthy of further research. At present, there is a paucity of studies in this field.

Funding Sources

This work was supported by the Zhejiang Provincial Natural Science Foundation of China (Grant No. LQ22E080024), the Natural Science Foundation Project of Liaoning Provincial Department of Education, China (Grant No. JJL201915404), the Zhejiang Province Department of Education Fund (Grant No. Y202146776) and the Natural Science Foundation of China (U2106219).

Authorship contribution statement

Zhiqiang Luo: Data curation, Writing- Original draft preparation, Methodology.
Huaxin Liu: Supervision, Writing- Reviewing & Editing, Investigation.
Genjin Liu: Writing-Review & editing, Conceptualization, Investigation, Validation.

Declaration conflict of interest

The authors of this article declare that they have no financial, professional or personal conflicts of interest that could have inappropriately influenced this work.

REFERENCES

1. Li J, Dong W, Zhao X, Li H. 2024. Investigation on fracture properties of concrete considering the viscoelastic characteristics. Constr. Build. Mater. 426:136044. https://doi.org/10.1016/j.conbuildmat.2024.136044
2. Son KS, Hajirasouliha I, Pilakoutas K. 2011. Strength and deformability of waste tyre rubber-filled reinforced concrete columns. Constr. Build. Mater. 25(1):218-226. https://doi.org/10.1016/j.conbuildmat.2010.06.035
3. Youssf O, ElGawady MA, Mills JE. 2015. Experimental investigation of crumb rubber concrete columns under seismic loading. Struct. 3:13-27. https://doi.org/10.1016/j.istruc.2015.02.005
4. Sukontasukkul P, Tiamlom K. 2012. Expansion under water and drying shrinkage of rubberized concrete mixed with crumb rubber with different size. Constr. Build. Mater. 29:520-526. https://doi.org/10.1016/j.conbuildmat.2011.07.032
5. Thomas BS, Gupta RC. 2015. Long term behaviour of cement concrete containing discarded tire rubber. J. Clean. Prod. 102:78-87. https://doi.org/10.1016/j.jclepro.2015.04.072
6. Gupta T, Siddique S, Sharma RK, Chaudhary S. 2019. Behaviour of waste rubber powder and hybrid rubber concrete in aggressive environment. Constr. Build. Mater. 217:283-291. https://doi.org/10.1016/j.conbuildmat.2019.05.080
7. Xue J, Shinozuka M. 2013. Rubberized concrete: A green structural material with enhanced energy-dissipation capability. Constr. Build. Mater. 42:196-204. https://doi.org/10.1016/j.conbuildmat.2013.01.005
8. Turatsinze A, Bonnet S, Granju JL. 2007. Potential of rubber aggregates to modify properties of cement based-mortars: improvement in cracking shrinkage resistance. Constr. Build. Mater. 21(1):176-181. https://doi.org/10.1016/j.conbuildmat.2005.06.036
9. He L, Cai H, Huang Y, Ma Y, Bergh WVD, Gaspar L, Valentin J, Vasiliev YE, Kowalski KJ, Zhang J. 2021. Research on the properties of rubber concrete containing surface-modified rubber powders. J. Build. Eng. 35:101991. https://doi.org/10.1016/j.jobe.2020.101991
10. Raffoul S, García R, Pilakoutas K, Guadagnini M, Medina NF. 2016. Optimisation of rubberised concrete with high rubber content: An experimental investigation. Constr. Build. Mater. 124:391-404. https://doi.org/10.1016/j.conbuildmat.2016.07.054
11. Shao J, Zhu H, Zuo X, Lei W, Borito SM, Liang J, Duan F. 2020. Effect of waste rubber particles on the mechanical performance and deformation properties of epoxy concrete for repair. Constr. Build. Mater. 241:118008. https://doi.org/10.1016/j.conbuildmat.2020.118008
12. Huang B, Li G, Pang SS, Eggers J. 2004. Investigation into waste tire rubber-filled concrete. J. Mater. Civ. Eng. 16(3):187-194. https://doi.org/10.1061/(ASCE)0899-1561(2004)16:3(187)
13. Issa CA, Salem G. 2013. Utilization of recycled crumb rubber as fine aggregates in concrete mix design. Constr. Build. Mater. 42:48-52. https://doi.org/10.1016/j.conbuildmat.2012.12.054
14. Liang T, Yang R, Zhao W. 2021. Research on stress resistance and strengthening mechanism of polyvinyl alcohol fiber concrete. Hi-tech. Fiber. Appl. (05):47-51. https://lib.cqvip.com/Qikan/Article/Detail?id=7105997155

15. Liu J, Zhang S, Zhou T. 2023. Influence of polyvinyl alcohol and ultrahigh molecular weight polyethylene fibers ondynamic mechanical properties of coral aggregate concrete and numerical simulation. Acta. Mater. Compos. Sin. 40(6): 3613-3625. https://fhclxb.buaa.edu.cn/article/doi/10.13801/j.cnki.fhclxb.20220901.002
16. Shao R, Wu C, Li J, Liu Z. 2023. Repeated impact resistance of steel fibre-reinforced dry UHPC: Effects of fibre length, mixing method, fly ash content and crumb rubber. Compos. Struct. 321:117274. https://doi.org/10.1016/j.compstruct.2023.117274
17. Vafaei D, Ma X, Hassanli R, Duan J, Zhuge Y. 2022. Microstructural behaviour and shrinkage properties of high-strength fiber-reinforced seawater sea-sand concrete. Constr. Build. Mater. 320:126222. https://doi.org/10.1016/j.conbuildmat.2021.126222
18. Wang J, Dai Q, Si R, Guo S. 2018. Investigation of properties and performances of Polyvinyl Alcohol (PVA) fiber-reinforced rubber concrete. Constr. Build. Mater. 193: 631-642. https://doi.org/10.1016/j.conbuildmat.2018.11.002
19. Noushini A, Vessalas K, Arabian G, Samali B. 2014. Drying shrinkage behaviour of fibre reinforced concrete incorporating polyvinyl alcohol fibres and fly ash. Adv. Civ. Eng. 2014(1):836173. https://doi.org/10.1155/2014/836173
20. Feng Y, Niu Z, Zhao C, Li L. 2023. Compressive test investigation and numerical simulation of polyvinyl-alcohol (PVA)-Fiber-Reinforced rubber concrete. Buildings. 13(2):431. https://doi.org/10.3390/buildings13020431
21. Teng S, Afroughsabet V, Ostertag CP. 2018. Flexural behavior and durability properties of high performance hybrid-fiber-reinforced concrete. Constr. Build. Mater. 182:504-515. https://doi.org/10.1016/j.conbuildmat.2018.06.158
22. Hamoush S, Abu-Lebdeh T, Cummins T. 2010. Deflection behavior of concrete beams reinforced with PVA micro-fibers. Constr. Build. Mater. 24(11):2285-2293. https://doi.org/10.1016/j.conbuildmat.2010.04.027
23. Noushini A, Vessalas K, Samali B. 2014. Static mechanical properties of polyvinyl alcohol fibre reinforced concrete (PVA-FRC). Mag. Concr. Res. 66(9):465-483. https://doi.org/10.1680/macr.13.00320
24. Mondoringin MR, Ohtsu M. 2013. Kinematics on split-tensile test of fiber-reinforced concrete by AE. J. Adv. Concr. Technol. 11(8):196-205. https://doi.org/10.3151/jact.11.196
25. Sagar B, Sivakumar MVN. 2021. Compressive properties and analytical modelling for stress-strain curves of polyvinyl alcohol fiber reinforced concrete. Constr. Build. Mater. 291:123192. https://doi.org/10.1016/j.conbuildmat.2021.123192
26. Cai XH, He Z, Liu W. 2014. Experimental study on impact resistance of PVA fiber reinforced cement-based composite. Appl. Mech. Mater. 584:1630-1634. https://doi.org/10.4028/www.scientific.net/AMM.584-586.1630
27. Chen W, Wen Y. 2024. Experimental study on mechanical and durability properties of concrete incorporating various polyvinyl alcohol fiber lengths and dosages. Mater. Construcc. 74(355):e349. https://doi.org/10.3989/mc.2024.368923
28. Kim DJ, Park SH, Ryu GS, Koh KT. 2011. Comparative flexural behavior of hybrid ultra high performance fiber reinforced concrete with different macro fibers. Constr. Build. Mater. 25(11):4144-4155. https://doi.org/10.1016/j.conbuildmat.2011.04.051
29. Shafiq N, Ayub T, Khan SU. 2016. Investigating the performance of PVA and basalt fibre reinforced beams subjected to flexural action. Compos. Struct. 153:30-41. https://doi.org/10.1016/j.compstruct.2016.06.008
30. Noushini A, Samali B, Vessalas K. 2013. Flexural toughness and ductility characteristics of polyvinyl-alcohol fibre reinforced concrete (PVA-FRC). In: Proceedings of the 8th International Conference on Fracture Mechanics of Concrete and Concrete Structures, FraMCoS 2013. Toledo, Spain. pp. 1110-1121. https://framcos.org/FraMCoS-8/p369.pdf
31. Xiao SH, Liao SJ, Zhong GQ, Guo YC, Lin JX, Xie ZH, Song Y. 2021. Dynamic properties of PVA short fiber reinforced low-calcium fly ash-slag geopolymer under an SHPB impact load. J. Build. Eng. 44:103220. https://doi.org/10.1016/j.jobe.2021.103220
32. Medina NF, Flores-Medina D, Hernández-Olivares F. 2016. Influence of fibers partially coated with rubber from tire recycling as aggregate on the acoustical properties of rubberized concrete. Constr. Build. Mater. 129:25-36. https://doi.org/10.1016/j.conbuildmat.2016.11.007
33. He W, Wu S, Zhang B, Liu Y, Luo Y, Fu G. 2023. Effect of fiber section shape and volume fraction on the mechanical properties of steel-fiber reinforced concretes. Mater. Construcc. 73(352):e328. https://doi.org/10.3989/mc.2023.350223
34. Isa MN, Pilakoutas K, Guadagnini M, Angelakopoulos H. 2020. Mechanical performance of affordable and eco-efficient ultra-high performance concrete (UHPC) containing recycled tyre steel fibres. Constr. Build. Mater. 255:119272. https://doi.org/10.1016/j.conbuildmat.2020.119272
35. Abaza OA, Hussein ZS. 2016. Flexural behavior of steel fiber-reinforced rubberized concrete. J. Mater. Civil. Eng. 28(1):04015076. https://doi.org/10.1061/(ASCE)MT.1943-5533.0001334
36. JGJ 55–2011. 2011. Specification for mix proportion design of ordinary concrete. Chinese Standard.
37. GB/T 50081–2019. 2019. Standard for test methods of physical and mechanical properties of concrete. Chinese Standard.
38. American Concrete Institute (ACI). 1996. ACI 544: Fiber reinforced concrete. Farmington Hills (MI): American Concrete Institute.
39. Uygunoğlu T, Topcu IB. 2010. The role of scrap rubber particles on the drying shrinkage and mechanical properties of self-consolidating mortars. Constr. Build. Mater. 24(7):1141-1150. https://doi.org/10.1016/j.conbuildmat.2009.12.027
40. Mohtasham Moein M, Saradar A, Rahmati K, Arman Shirkouh H, Sadrinejad I, Aramali V, Karakouzian M. 2022. Investigation of impact resistance of high-strength portland cement concrete containing steel fibers. Mater. 15(20):7157. https://doi.org/10.3390/ma15207157
41. Rahmani T, Kiani B, Shekarchi M, Safari A. 2012. Statistical and experimental analysis on the behavior of fiber reinforced concretes subjected to drop weight test. Constr. Build. Mater. 37:360-369. https://doi.org/10.1016/j.conbuildmat.2012.07.068
42. Ostle B, Tumer KV, Hicks CR. 1996. Engineering statistics: the industrial experience. New York: Duxbury Press.
43. Binici B. 2008. Design of FRPs in circular bridge column retrofits for ductility enhancement. Eng. Struct. 30(3):766-776. https://doi.org/10.1016/j.engstruct.2007.05.012
44. Chen J, Yuan Y, Zhu Q, Duan J. 2023. High-temperature resistance of high-strength concrete with iron tailing sand. J. Build. Eng. 63:105544. https://doi.org/10.1016/j.jobe.2022.105544